



## A late proterozoic–early paleozoic magmatic cycle in Sierra de la Ventana, Argentina

D.A. Gregori<sup>a,\*</sup>, V.L. López<sup>a</sup>, L.E. Grecco<sup>b</sup>

<sup>a</sup>CONICET and Cátedra de Geología Argentina, Departamento de Geología, Universidad Nacional del Sur, San Juan 670, 8000 Bahía Blanca, Argentina  
<sup>b</sup>CONICET and Cátedra de Geoquímica, Departamento de Geología, Universidad Nacional del Sur, San Juan 670, 8000 Bahía Blanca, Argentina

Received 1 October 2003; accepted 31 October 2003

### Abstract

Late Proterozoic–Early paleozoic intrusive and volcanic rocks of Sierra de la Ventana can be grouped into two magmatic assemblages: the Meyer and Cochenleufú suites. The older Meyer suite (700–570 Ma) is composed of S-type quartz-monzonodiorites, syngranites, and monzogranites associated with andesites and rhyolites and related to volcanic arc and postcollisional settings. The younger Cochenleufú (540–470 Ma) corresponds to highly fractionated homogeneous A-type monzogranites, linked to final plutonic events during postorogenic extension in collisional belts. Strong similarities between Sierra de la Ventana magmatic rocks and the S- and A-type granites of the Cape granite suite in South Africa allow for positive correlation. In both areas, primitive volcanic arcs or collisional orogens are recognized. Continuous transpressional shearing between the Swartland and Tygerberg terranes in the Saldania belt may have triggered the generation and emplacement of both suites.

© 2003 Published by Elsevier Ltd.

**Keywords:** Argentina; Late proterozoic–Early paleozoic magmatism; Sierra de la ventana

### 1. Introduction

Located in southeastern Buenos Aires province, Argentina, Sierra de la Ventana is a 180 km long sigmoidal mountain belt, composed of basement and sedimentary cover (Fig. 1). The basement consists of Late Precambrian–Early Paleozoic deformed granites, rhyolites, and andesites. The Paleozoic sedimentary sequences can be divided into three groups. Conglomerates and quartzites compose the Curamala (Ordovician–Silurian) and Ventana (Silurian–Devonian) Groups. The Pillahuincó Group (Upper Carboniferous–Permian) is composed of glacial deposits, black shales, and sandstones. Deformational episodes occurred during the Upper Devonian and Permian.

Keidel (1916) correlated the Sierra de la Ventana sequences with the Karoo basin in South Africa, and Du Toit (1937) integrated both areas in the Samfrau geosyncline. Andreis (1964), Andreis et al. (1989), Borrello (1962) and (1964), Buggisch (1987), Harrington (1947), (1970), (1972) and (1980), Iñiguez Rodríguez and Andreis

(1971), Kilmurray (1968a,b) and (1975), Kilmurray et al. (1985), Llambías and Prozzi (1975), Sellés Martínez (1989), Varela (1973) and (1978) and von Gosen et al. (1990), (1991) and (2002), among others, carried out geological studies in Sierra de la Ventana. In addition, Grecco et al. (1984) and (1999), Grecco and Gregori (1993), Varela (1985), Rapela and Pankhurst (2002), and Rapela et al. (2001) and (2003) studied its petrography, geochemistry, and geochronology and reported preliminary geotectonic interpretations of the igneous rocks.

In this paper, we present new petrographical and geochemical data about the intrusive and volcanic rocks of Sierra de la Ventana. These are integrated with regional geological data to postulate the magmatic source of the rocks and propose a model for the Late Proterozoic–Early paleozoic tectonomagmatic evolution of this part of Gondwana.

### 2. Field relationships and petrography of the igneous rocks

Igneous rocks crop out at La Mascota, La Ermita, Agua Blanca, Pan de Azucar, Cerro del Corral, San Mario, and

\* Corresponding author. Tel.: +54-291-459-5101 ext. 3030.  
 E-mail address: usgregor@criba.edu.ar (D.A. Gregori).

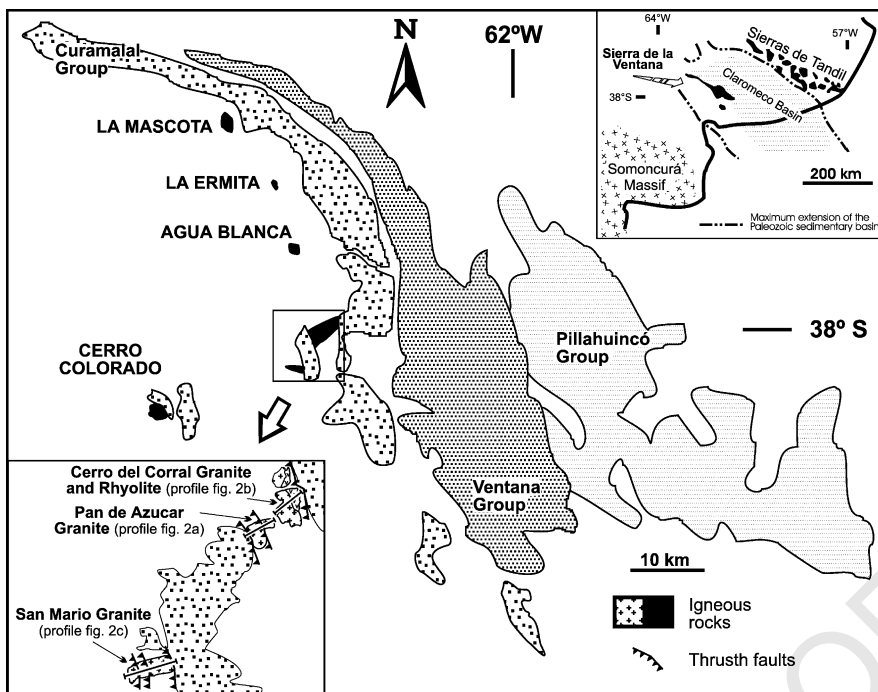
113  
114  
115  
116  
117  
118  
119  
120  
121  
122  
123  
124  
125  
126  
127  
128  
129  
130  
131  
132  
133  
134

Fig. 1. Major tectonic domains in SE Buenos Aires. The box in the upper right hand shows the location of Sierra de la Ventana, as expanded in the main area of the figure. The location of the studied igneous rocks is clarified in the lower left-hand box.

Cerro Colorado (Fig. 1). Most are exposed on the western side of the Sierra de la Ventana due to tectonic transport to the northeast by thrust faults (Cobbold et al., 1986). The outcrops at Cerro Colorado, La Ermita, and Agua Blanca are granitic and rhyolitic rocks overlain by Quaternary sediments. Those at San Mario, Pan de Azucar, and Cerro del Corral show tectonic contacts with the Paleozoic sedimentary cover (Fig. 1).

According to field relationships in the San Mario, Pan de Azucar, and Cerro del Corral granites, as well as in the Cerro del Corral rhyolite and the Pan de Azucar andesite, these rocks can be grouped into the Meyer suite. Strong ductile deformation and a typical geochemical signature, as reported subsequently, characterize this suite.

The Cochenleufú suite consists of the Agua Blanca and Cerro Colorado granites and the La Ermita rhyolite. They are slightly deformed and characterized by a distinctive magmatic fabric.

### 2.1. Meyer suite

#### 2.1.1. Pan de Azucar

In Pan de Azucar (Fig. 2a), the greenschists, metaquartzites, basic bodies, and mylonitized granites described by Cuerda et al. (1975) underlie the Paleozoic sequence (Pan de Azucar Formation). Schiller (1930) and Cucchi (1966) infer a tectonic contact, whereas von Gosen et al. (1990) find no evidence of intrusive contact. Cobbold et al. (1986) suggest a dextral overthrust to the northeast. Our interpretation, based on the presence of ultramylonitic belts ( $344^{\circ}/61^{\circ}\text{SW}$ ) in the granitic rocks, is a NE-vergent overthrust.

As shown in Fig. 2a, the eastern flank of the Cerro Pan de Azucar consists of deformed plutonic and volcanic rocks. Plutonic rocks exhibit isograngular to ultramylonitic textures. The former are composed of quartz, twinned K-feldspar, plagioclase ( $\text{An}_{26-33}$ ), and biotite. Plagioclase is replaced by sericite, epidote, and calcite. In the QAP modal triangle (Fig. 2a), these rocks plot in the syngranite and monzogranite fields. In protoclastic and protomylonitic varieties, quartz, plagioclase, and K-feldspar were disrupted to produce porphyroclasts with patchy extinction and fracturing. In the mylonitic granites, a fine-grained matrix composed of quartz, biotite, sericite, and chlorite wraps around rotated porphyroclasts of quartz, plagioclase, and K-feldspar. The ultramylonitic granites display a few strongly fractured porphyroclasts of K-feldspar in a fine-grained matrix of quartz, muscovite, and chlorite with minor calcite and biotite.

Basic and acidic volcanic rocks also are recognized in this profile. Acidic rocks consist of a 1 m thick belt of porphyritic rocks with 30% euhedral quartz, plagioclase ( $\text{An}_{10-15}$ ), and K-feldspar fenocrysts in a groundmass of microcrystalline quartz, alkaline feldspar, and fine micas. Quartz shows embayment, whereas plagioclase contains agglomerates. Its microscopic characteristics and QAP diagram classification correspond with a rhyolite.

Basic vulcanites appear as a 10 m thick, 90 m long body with notable coarse fenocrysts of plagioclase. Kilmurray (1968b) first described these rocks as diabases. The groundmass displays a pilotaxitic texture with laths of plagioclase and elongated crystals of tremolite, epidote, and quartz. The plagioclase ( $\text{An}_{20-23}$ ) shows alteration to

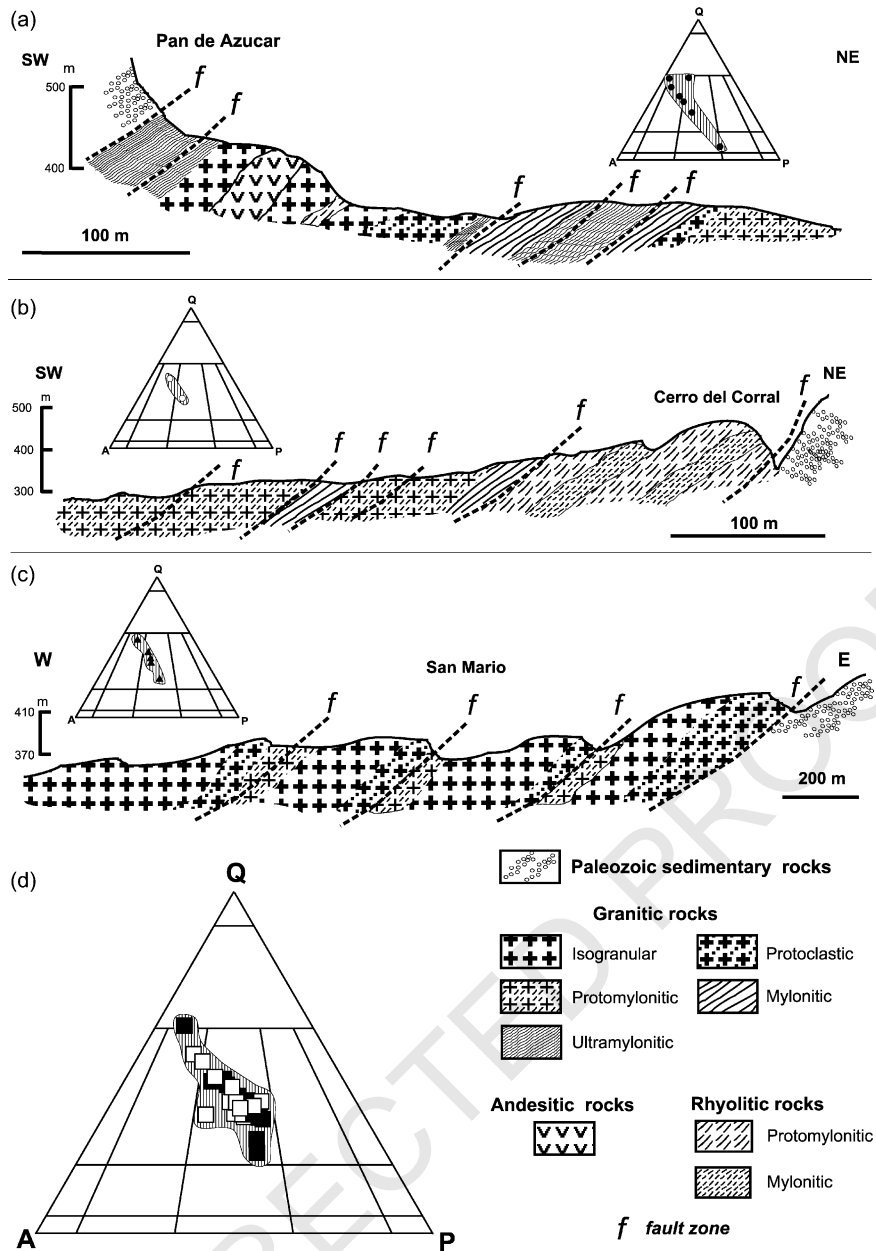


Fig. 2. Profiles at (a) Pan de Azucar, (b) Cerro del Corral, and (c) San Mario. (d) QAP diagram for the Cochenleufú suite.

epidote and sericite. Oscillatory zoning and lamellar twinning are common. On the basis of these characteristics, the rocks are classified as andesites.

#### 2.1.2. Cerro del corral

Cerro del Corral is located 100 m east of Pan de Azucar, and together they constitute the core of a large overturned anticline. Ductile shear zones and belts of mylonites and phyllonites on the eastern side of Cerro del Corral are related to overthrusting on the Paleozoic sequences. Protoclastic, protomylonitic, and mylonitic granites appear on the western flank of the Cerro del Corral (Fig. 2b). They are coarse- to medium-sized grains with fractured quartz, K-feldspar, and twinned

plagioclase ( $An_{8-10}$ ). Secondary quartz, biotite, and muscovite appear in veinlets or disseminated crystals. On a QAP diagram, these rocks plot in the syngranite and monzogranite fields.

Volcanic rocks display porphyritic, protomylonitic, and mylonitic textures. Porphyritic varieties are composed of 20% quartz, alkali feldspar, and plagioclase phenocrysts. Quartz appears as subhedral phenocrysts with embayment and shadowy extinction. The alkali feldspars are euhedral and exhibit simple twinning and flame-like pertites. The scarce plagioclase phenocrysts ( $An_{10-12}$ ) have diffuse lamellar twinning. The matrix consists of muscovite, biotite, calcite, subhedral quartz, and plagioclase ( $An_{10}$ ). They are petrographically classified as rhyolites.

337 Micaceous-rich, coarse bands of quartz and alkali  
 338 feldspar compose the mylonitized rhyolites. The original  
 339 igneous quartz and alkali feldspar represent porphyroclasts  
 340 or augens surrounded by a deformed matrix.

### 341 2.1.3. Cerro San Mario

342 In San Mario, an E–W, elongated, granitic body (600 m  
 343 long, 150 m wide) is overthrust on conglomerates of the  
 344 Curamal Group. The San Mario granite is a medium- to  
 345 coarse-grained biotite monzogranite with protoclastic to  
 346 protomylonitic textures (Fig. 2c). The mineralogy consists  
 347 of quartz, K-feldspar, plagioclase, and biotite. Plagioclase  
 348 ranges from An<sub>15–33</sub> in syngranites to An<sub>26–40</sub> in  
 349 monzogranites. Large alkali feldspar is usually perthitic  
 350 and shows shadowy, crosshatched twinning.

351 Several foliated belts cut the granite N–S (353°/66°SW).  
 352 Minor aplite and pegmatite dikes crosscut the granites.  
 353 Delpino and Dimieri (1992) recognize two deformational  
 354 events. The first is evidenced by a regional NNW  
 355 schistosity, and NE shear planes represent the second.

### 356 2.2. Cochenleufú diutie

#### 357 2.2.1. Agua blanca

358 The Agua Blanca granite occurs 10 km north of Pan de  
 359 Azucar It is a porphyritic to aplitic granite, composed of  
 360 microcline, anorthoclase, quartz, and plagioclase.  
 361 Quartz appears as isolated phenocrysts, whereas plagioclase  
 362 (An<sub>0–5</sub>) is subhedral to euhedral. Biotite with strong  
 363 pleocroism and muscovite are scarce. Fluorite is present  
 364 as disseminated crystals or veinlets in the microcline  
 365 (Grecco, 1990). Most samples from the Agua Blanca  
 366 granite plot on the monzogranite field in a QAP diagram  
 367 (Fig. 2d). Dimieri et al. (1990) describe kink bands,  
 368 deformational twinning, and flexures in microcline and  
 369 biotite crystals, which suggests ductile deformation during  
 370 the solid-state stage (Simpson, 1985; Paterson et al., 1989).

#### 371 2.2.2. La Ermita

372 La Ermita is located 10 km NNW of Agua Blanca It  
 373 consists of a N–S, 500 m long hill with no relationship to  
 374 the Paleozoic cover. These rocks display fluidal and  
 375 microporphyritic textures with quartz and K-feldspar  
 376 phenocrysts. Quartz is anhedral and presents undulose  
 377 extinction and parallel deformational bands. The ground-  
 378 mass is completely recrystallized to fine-grained quartz.  
 379 Fluorite and iron oxides appear as disseminated crystals.  
 380 These rocks are classified as rhyolites.

#### 381 2.2.3. Cerro colorado

382 Cerro Colorado is located 20 km W of Cerro San Mario  
 383 The predominant lithology is a medium to coarse granite  
 384 (Fig. 2d). Microcline, quartz, and plagioclase are the most  
 385 abundant minerals; biotite, muscovite, fluorite, zircon,  
 386 apatite, and magnetite are accessory minerals. Quartz  
 387 appears as small to medium clusters between the microcline

388 or as large phenocrysts. Microcline appears as large  
 389 (3–5 cm) euhedral to subhedral crystals. Plagioclase  
 390 (An<sub>6–10</sub>) is euhedral with crystals up to 10 mm long, often  
 391 twinned with albite and albite-carlsbad. Micaceous minerals  
 392 are pleochroic biotite and kink-banded muscovite flakes.  
 393 Fluorite appears as disseminated crystals in K-feldspar,  
 394 irregular veinlets, and small lenses.

395 The western side of Cerro Colorado contains a foliation  
 396 marked by the orientation of K-feldspar megacrysts  
 397 (3–5 cm long) and mica flakes. The K-feldspar megacrysts  
 398 are aligned in two trends: L1 (55–65°/N300–120°) and L2  
 399 (55–65°/N20–200°). Biotites display a 289°/44°SW to  
 400 340°/35°SW foliation. Biotite cumulates also follow this  
 401 foliation. Orientations of feldspar and micas form an angle  
 402 of 20–40° and display a S–C foliation. This fabric was  
 403 developed during a submagmatic stage (Miller and  
 404 Paterson, 1994; Tribe and D'Lemos, 1996). Dimieri et al.  
 405 (1990) describe similar features in the Agua Blanca granite.

### 406 3. Geochemistry systematics

407 Major, trace, and rare earth elements (REE) geochemical  
 408 data for both suites appear in Tables 1 and 2. X-ray  
 409 fluorescence was used to determine major, minor, and trace  
 410 elements: SiO<sub>2</sub>, TiO<sub>2</sub>, Al<sub>2</sub>O<sub>3</sub>, FeO, MnO, MgO, CaO, Na<sub>2</sub>O,  
 411 K<sub>2</sub>O, P<sub>2</sub>O<sub>5</sub>, Ba, Cl, Co, Cr, Cu, Ga, Nb, Pb, Rb, Sr, Th, U, V,  
 412 Y, Zn, and Zr. International geostandards, including AC–E,  
 413 MA–N, GS–N, GA, and GH granitoids, were used for  
 414 instrumental calibration. The analyses were carried out at  
 415 University of Barcelona. Instrumental neutron activation  
 416 analyses were carried out on 31 selected samples to  
 417 determine the REE, Ta, Hf, Sc, Cs, and Sn at ACTLABS.

#### 418 3.1. Meyer suite

##### 419 3.1.1. Major elements

420 The granitoids of the Meyer suite are the most mafic  
 421 of the Sierra de la Ventana igneous rocks, ranging in  
 422 composition from monzonite to granite (Table 1) Harker  
 423 diagrams of major elements display decreasing TiO<sub>2</sub>,  
 424 Al<sub>2</sub>O<sub>3</sub>, Fe<sub>2</sub>O<sub>3</sub>, MgO (Fig 3a–d), and CaO and increasing  
 425 K<sub>2</sub>O with increasing fractionation, thus implying a  
 426 comagmatic origin for these rocks. SiO<sub>2</sub> concentrations  
 427 are between 57 and 77 wt% in the Pan de Azucar  
 428 granite, 67–76 wt% in the Cerro del Corral granite, and  
 429 68–76 wt% in San Mario. The granitoids are character-  
 430 ized by high K<sub>2</sub>O (Cerro del Corral and Pan de Azucar:  
 431 6.29 wt%, San Mario: 5.28 wt%) and fall in the  
 432 shoshonitic and high-K calc-alkaline fields of Pecerrillo  
 433 and Taylor (1976) classification.

434 The AFM diagram (not shown) indicates a calc-alkaline  
 435 evolution, with A ranging from 55 to 85 and evolving from  
 436 the Pan de Azucar andesite to the Cerro del Corral rhyolite.  
 437 The granitic rocks occupy the transitional terms of this  
 438 series. All samples are subalkaline.

Table 1  
Chemical analyses of the Meyer suite (major elements in w%, trace, and REE in ppm)

Sample	CR0590	CR0190	PA 0991	PA 0491	PA0891	PA2191	PA2291	PA1891	PA0291	PA0791	PA1691	SM 0292	SM 0492	SMO2	SM 0192	SM 0392	PA 1991	CR0791	CR0690	CR0391
Locality	Corral granite	Pan Azucar										San Mario					Azucar Andesite	Corral Rhyolite		
SiO <sub>2</sub>	67.96	68.44	72.93	72.54	74.81	61.59	60.75	57.01	67.53	69.93	65.05	68.36	76.09	72.89	70.67	68.21	60.71	76.49	74.58	73.05
TiO <sub>2</sub>	0.68	0.54	0.56	0.52	0.35	0.55	0.63	0.91	0.43	0.73	0.80	0.33	0.21	0.27	0.30	0.52	0.78	0.09	0.07	0.07
Al <sub>2</sub> O <sub>3</sub>	16.47	15.37	15.79	16.26	13.98	15.85	15.79	17.44	15.91	15.81	16.29	15.51	14.75	14.78	15.16	16.35	16.41	13.36	13.01	17.15
FeO	4.24	2.80	1.99	1.60	1.35	4.28	4.30	6.45	4.42	2.66	3.56	2.34	1.08	1.19	1.94	3.05	5.81	0.78	1.11	1.46
MnO	0.05	0.04	0.02	0.02	0.03	0.14	0.11	0.24	0.15	0.03	0.04	0.06	0.01	0.03	0.06	0.05	0.25	0.07	0.02	0.01
MgO	1.27	0.92	0.76	0.63	0.78	2.05	2.10	1.51	1.43	1.18	1.32	0.49	0.38	0.34	0.76	1.35	1.46	0.13	0.06	0.44
CaO	0.67	0.46	0.13	0.32	1.73	1.82	1.68	1.79	2.05	0.56	2.32	1.52	0.24	0.89	0.87	3.15	2.88	1.23	0.24	0.00
Na <sub>2</sub> O	0.87	2.50	0.77	0.14	0.57	4.59	6.99	3.89	0.26	1.75	1.57	3.24	1.02	2.23	2.40	0.31	0.10	0.34	3.60	0.24
K <sub>2</sub> O	4.91	5.32	5.95	5.59	3.99	4.35	4.04	6.29	5.13	5.50	5.12	5.28	5.21	5.11	5.10	4.53	6.05	4.89	5.10	4.91
P <sub>2</sub> O <sub>5</sub>	0.24	0.17	0.17	0.09	0.09	0.16	0.18	0.14	0.05	0.12	0.20	0.13	0.06	0.05	0.13	0.06	0.10	0.01	0.02	0.02
LOI	1.93	2.93	1.37	2.00	2.34	3.12	2.06	3.45	1.98	1.32	3.00	2.32	1.82	1.57	1.18	1.90	4.74	1.89	1.19	2.05
Cr	8	10	5	5	17	27					23	18	13	21	14	48	410	6	2	12
Co	44	57	55	72	73	46					64	67	86	104	53	87	34	83	110	47
Sc	11	4	3	5	2	10					6	4	3	5	4	25	4	4	3	
V	45	41	23	30	24	65	65	121	38	47	68	27	8	15	20	63	119	1	2	8
Rb	170	208	192	179	107	109	83	284	167	197	166	205	177	220	174	149	266	1.00	1.00	1.00
Cs	2.00	2.00	22.00	1.00	2.00	3.00					3.00	3.00	1.00	3.00	4.00	9.00	274	285	555	
Ba	1441	1073	794	1416	460	650	652	1169	765	753	1064	1177	752	579	1201	427	1026	102	56	20
Sr	105	143	170	238	161	410	356	38	82	191	191	122	99	98	223	216	60	20	21	16
Ga	18	21	16	16	14	19	20	18	15	16	21	17	15	17	17	19	15	3.20	4.00	2.00
Ta	0.50	1.00	4.98	5.50	1.00	2.00					4.00	4.98	5.00	3.04	0.50	5.53	8.86	25.3	40.9	24.6
Nb	22.9	17.3	9.4	13.8	11.0	14.2	15.3	18.8	18.8	1.4	15.6	21.7	23.7	25.6	17.9	17.1	18.0	7.00	8.00	5.00
Hf	10.00	8.00	9.00	12.00	5.00	6.00					10.00	5.00	5.00	7.00	7.00	6.00	153	148	97	
Zr	291	200	265	386	243	180	171	113	166	420	254	181	137	145	232	177	109	37	80	23
Y	27	9	19	22	11	10	11	21	36	21	11	22	24	31	18	11	18	26.34	41.48	18.55
Th	8.20	21.12	95.19	61.09	61.58	5.80	7.88	3.84	11.07	142.17	24.42	13.37	18.01	25.19	10.42	17.67	4.23	1.30	8.19	3.75
U	0.20	0.40	1.40	1.10	1.93	0.40					1.2	2.30	1.11	2.60	0.40		1.10	38.00	22.00	19.00
La	49.00	34.00	150.00	120.00	94.00	30.00					80.00	37.00	38.00	51.00	44.00		21.00	75.00	53.00	35.00
Ce	88.00	77.00	240.00	210.00	170.00	54.00					150.00	65.00	67.00	81.00	81.00		38.00	38.00	34.00	14.00
Nd	45.00	30.00	130.00	96.00	81.00	22.00					61.00	22.00	32.00	35.00	34.00		15.00	6.40	8.20	2.50
Sm	7.00	4.60	16.00	11.00	10.00	4.20					9.60	3.70	4.50	6.00	3.90		3.80	0.20	0.20	0.40
Eu	1.40	0.60	0.90	1.30	1.10	1.40					1.50	0.80	0.90	1.00	1.00		1.10	1.20	1.90	0.60
Tb	1.00	0.50	0.41	0.50	0.50	0.40					0.48	0.50	0.50	0.40	0.50		0.80	5.05	9.06	3.07
Yb	3.83	1.20	1.64	3.51	0.92	1.54					1.21	3.22	4.01	5.43	2.66		3.21	0.67	1.27	0.45
Lu	0.61	0.13	0.20	0.54	0.10	0.20					0.16	0.49	0.53	0.70	0.46		0.42	6.54	6.51	19.71
Cl	b.d.	40.47	14.20	14.26	13.06	26.47	27.08	7.12	11.05	33.57	18.47	17.07	58.96	97.90	32.39	26.96	17.68			

Table 2  
Chemical analyses of the Cochenleufú suite (major elements in w%, trace, and REE in ppm)

Sample Locality	AB 02 Agua Blanca	AB 09	AB 15	AB 14	AB 03	AB 17 g	AB 1884	AB 2284	AB 17r	AB 1722	AB 1384	AB 0884	AB 0384	CC 02 Cerro Colorado	CC 04	CC 05	CC 08
SiO <sub>2</sub>	75.89	74.33	75.31	73.26	74.35	75.33	76.32	74.37	74.18	76.37	73.03	77.01	76.23	77.18	77.36	75.49	76.09
TiO <sub>2</sub>	0.04	0.05	0.03	0.12	0.02	0.05	0.02	0.02	0.05	0.02	0.05	0.02	0.06	0.08	0.11	0.10	0.11
Al <sub>2</sub> O <sub>3</sub>	12.85	13.95	13.29	14.30	13.29	13.89	13.36	12.94	13.35	13.77	13.64	13.84	13.84	11.95	11.63	12.99	12.34
FeO	1.35	1.09	1.63	1.01	1.29	1.75	0.36	0.91	1.25	0.77	1.20	0.49	0.63	0.85	0.93	1.04	1.22
MnO	0.23	0.19	0.10	0.08	0.09	0.49	0.33	0.10	0.49	0.09	0.11	0.08	0.04	0.01	0.01	0.01	0.03
MgO	0.15	0.04	0.42	0.03	0.06	0.19	0.02	0.01	0.11	0.01	0.12	0.06	0.09	0.10	0.10	0.10	0.10
CaO	0.70	0.10	0.21	0.70	0.90	0.16	0.29	0.37	0.13	0.39	0.15	0.11	0.50	0.10	0.17	0.26	0.28
Na <sub>2</sub> O	3.20	4.43	4.34	4.22	3.79	3.68	2.37	6.00	3.68	0.59	5.46	2.80	2.75	3.27	3.17	3.65	3.48
K <sub>2</sub> O	4.64	4.26	4.20	4.14	4.45	4.26	5.33	4.80	4.26	4.82	5.10	4.76	4.79	5.73	4.68	5.25	4.88
P <sub>2</sub> O <sub>5</sub>	0.03	0.03	0.01	0.02	0.01	0.01	0.00	0.00	0.01	0.00	0.00	0.01	0.01	0.01	0.02	0.01	0.02
LOI	0.87	0.50	0.52	0.40	0.60	0.21	1.54	0.25	0.50	0.64	0.45	0.63	0.79	0.62	0.27	0.32	0.32
Cr							350			15	47	360		310			
Co							4			97	78	3	4				
Sc										3	10	17	6	5			
V										4	1	9	4	1			
Rb											773	558	533	455			
Cs											23.00	3.00	6.00	5.00			
Ba											240	47	170	30			
Sr											27	2	8	5			
Ga											15	28	22	24			
Ta											5.00	7.93	4.00	4.00			
Nb											51.0	58.5	52.3	52.9			
Hf											3.00	16.00	14.00	6.00			
Zr											74	152	132	85	67	75	
Y											64	150	101	184	87	169	93
Th											29.46	42.95	15.00	45.83	52.92	24.85	62.48
U											3.14		4.50	4.10	4.00	2.00	3.50
La												18.00	14.00	110.00	13.00	16.00	
Ce												49.00	54.00	170.00	33.00	37.00	
Nd												17.00	16.00	71.00	25.00	23.00	
Sm												6.70	9.40	13.00	7.70	7.60	
Eu												0.20	0.20	3.10	0.30	0.20	
Tb												2.10	2.60	0.20	2.20	1.80	
Yb												10.90	29.70	3.59	18.70	11.60	
Lu												1.32	3.90	0.53	2.73	1.66	
Cl												100.70	30.68	31.40	35.01	33.59	68.00
																	39.58
Sample Locality	CC 20 Cerro Colorado	CC 23	CC 24	CC 26	CC 1683	CC 1983	CC 2283	CC 3183	CC 0183	CC 02b	CC 03						
SiO <sub>2</sub>	76.45	74.01	74.75	76.91	75.98	76.59	77.40	77.50	77.80	74.27	76.18						
TiO <sub>2</sub>	0.06	0.06	0.08	0.04	0.09	0.07	0.06	0.06	0.10	0.08	0.05						
Al <sub>2</sub> O <sub>3</sub>	12.29	13.32	13.65	12.75	13.05	13.05	13.56	12.86	13.37	13.07	12.52						
FeO	0.86	1.40	1.22	0.43	1.16	0.77	0.89	0.99	1.13	1.17	1.22						
MnO	0.01	0.01	0.01	0.01	0.03	0.01	0.01	0.02	0.01	0.01	0.01						
MgO	0.10	0.06	0.09	0.20	0.09	0.07	0.05	0.03	0.22	0.12	0.01						
CaO	0.10	0.87	0.50	0.54	0.38	0.59	0.40	0.32	0.10	0.10	0.46						
Na <sub>2</sub> O	4.00	3.49	3.83	3.97	3.22	3.58	1.71	2.40	1.50	2.90	4.07						
K <sub>2</sub> O	4.83	4.88	4.91	4.33	5.12	4.96	5.17	5.12	5.30	6.36	3.84						
P <sub>2</sub> O <sub>5</sub>	0.02	0.02	0.02	0.02	0.01	0.01	0.00	0.00	0.01	0.02	0.01						
LOI	0.10	0.51	0.21	0.37	0.68	0.17	0.64	0.53	0.32	0.32	0.19						
Cr					2	3	6	5	4								
Co					4	3	3	1	4								
Sc					4	4	4	3	5								
V					10	5	6	2	2								
Rb					394	423	467	262	352								
Cs					17.00	17.00	9.00	5.00	9.00								
Ba					67	51	45	140	126								
Sr					8	7	9	16	7								
Ga					23	24	24	19	20								
Ta					3.00	5.00	4.00	3.00	2.00								

The ASI index ranges 0.83–2.3 for the Cerro Corral and Pan de Azucar granites and 1.9–1.1 for San Mario; for the Pan de Azucar andesite, it is 1.3, and for the Cerro del Corral rhyolites, it ranges 1.0–3.0. This range plots in the peraluminous field on Shand (1943) diagram (not shown).

The normative corundum reaches 8.9% in the Cerro del Corral granite, 9.4% in Pan de Azucar, and 7.1% in San Mario, though modal corundum was not recognized. On the basis of their petrographical and geochemical characteristics, the Cerro del Corral, Pan de Azucar, and San Mario granites are interpreted as S-types. The Cerro de Corral rhyolites plot in the peraluminous field of Shand (1943) diagram and in the banakite and high-K rhyolite field of Pecerrillo and Taylor (1976) classification.

### 3.1.2. Trace and REE

Granites of the Meyer suite display significant variations in trace element contents (Table 1) Fractional crystallization is well represented by the K/Rb ratio, which decreases from 401 to 184 in the Pan de Azucar granite, from 261 to 189 in the Cerro del Corral granite, and from 252 to 197 in the San Mario granite. With increasing fractionation, Ba, Sc, Mn, and Zr decrease and Ga, Ta, Nb, and Y increase (Fig. 3e–h). This indicates fractional crystallization of plagioclase and K-feldspar in the melt, with enrichment of Rb and depletion of Sr in later stages (Grecco et al., 1999).

The total REE reaches 539 ppm in Pan de Azucar, 195 ppm in Cerro del Corral, and 180 ppm in San Mario. Chondrite-normalized spider diagrams of Pan de Azucar (Fig. 4a) indicate strong enrichment of LREE. The La<sub>N</sub>/Lu<sub>N</sub> between 16 and 100 suggests that garnet remained as a residual phase during the melting of the parental rocks.

The patterns for Cerro del Corral (Fig. 4b) also display important LREE enrichments, though not as high as those of Pan de Azucar. Their  $\text{La}_N/\text{Lu}_N$  relationships vary between 8.6 and 28.0 with small Eu anomalies, reflecting some plagioclase fractionation. San Mario displays patterns similar to those of Cerro del Corral, with  $\text{La}_N/\text{Lu}_N$  relationships varying between 7.6 and 10.2 (Fig. 4c).

The Pan de Azucar andesite is classified by Winchester and Floyd (1977) as andesite and alkaline basalt. The total REE concentration reaches 83 ppm, with  $\text{La}_N/\text{Lu}_N$  of 5.35 and  $\text{Eu}/\text{Eu}^*$  of 0.82 (Fig. 4d). 768  
769  
770  
771

The Cerro del Corral rhyolite has a high concentration of silica and alkalies, thus classifying it as a high-K subalkaline (Leat et al., 1986). The total REE concentration reaches 164 ppm. Chondrite-normalized diagrams (Fig. 4b) display severe negative Eu anomalies ( $\text{Eu/Eu}^*$ : 0.097–0.42), which indicate that plagioclase was strongly fractionated.

### 3.2. *Cochenleufú suite*

### *3.2.1. Major elements*

The Agua Blanca and Cerro Colorado granites present very restricted chemical compositions (**Table 2**) with

	Nb	Hf	Ta	Tb	Yb	Lu	Cl
40.9	46.8	46.2	39.1	37.1	29.0		
11.00	10.00	7.00	4.00	6.00			
140	121	79	34	104	107		
96	129	98	77	53	79		
66.17	64.18	46.37	53.75	33.26			
4.06	9.66	3.50	1.90	3.30			
29.00	26.00	19.00	15.00	39.00			
77.00	79.00	53.00	43.00	81.00			
34.00	30.00	22.00	23.00	39.00			
12.00	14.00	9.30	9.80	9.00			
0.30	0.40	0.20	0.20	0.40			
3.20	3.40	2.70	2.20	1.90			
13.90	18.20	12.90	10.30	6.13			
1.67	2.26	1.67	1.26	0.88			
32.87	33.28	32.75	30.27	35.15			

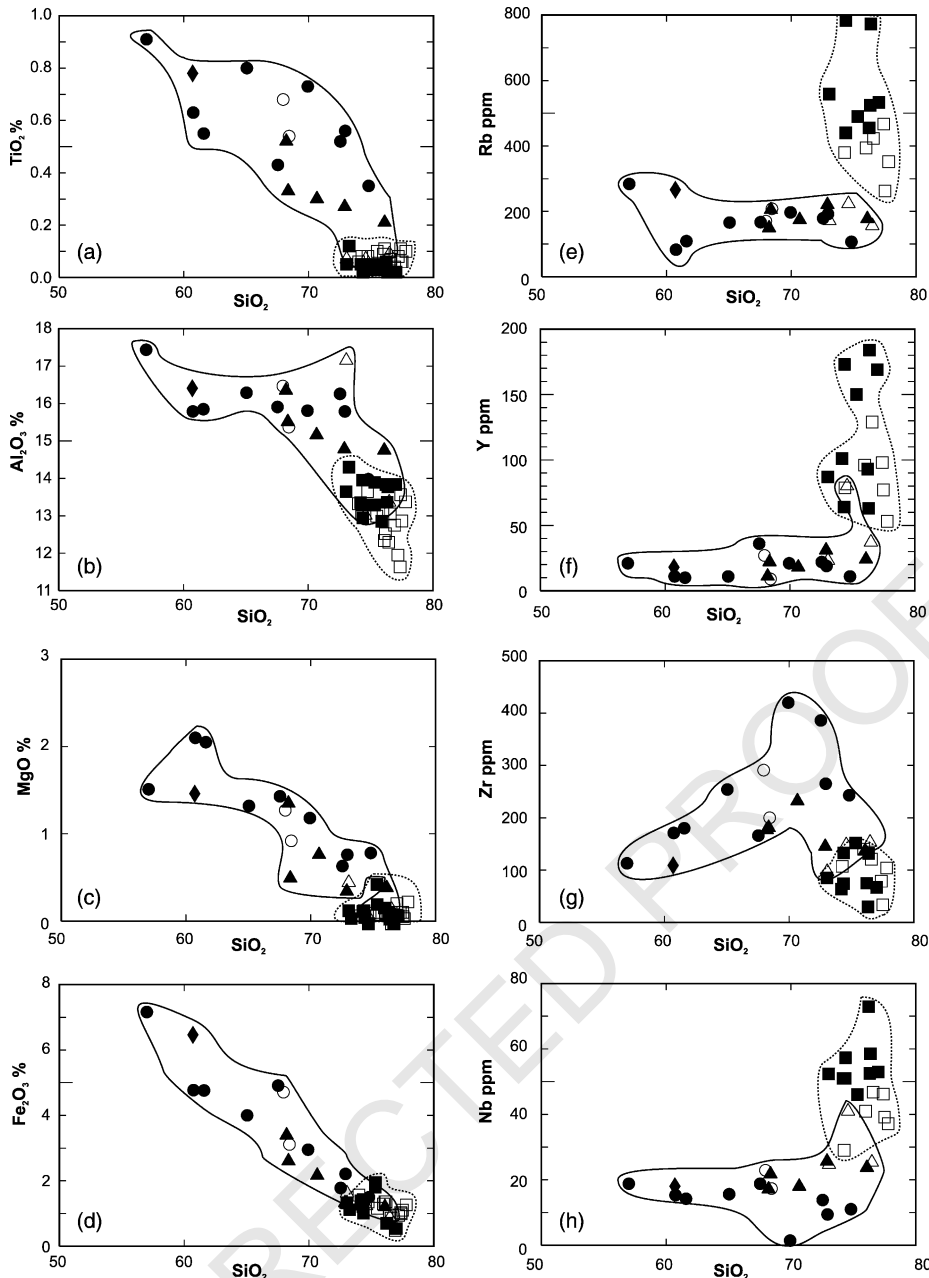


Fig. 3. Harker diagrams for the Meyer and Cochenleufú suites. Pan de Azucar granite •, Cerro del Corral granite ●, San Mario granite ▲, Cerro del Corral rhyolite △, Pan de Azucar andesite ♦, Agua Blanca granite □, and Cerro Colorado granite □.

$\text{SiO}_2 = 73\text{--}77 \text{ wt}\%$ ,  $\text{Al}_2\text{O}_3 = 11\text{--}17 \text{ wt}\%$ , and  $\text{K}_2\text{O} = 3.84\text{--}6.36 \text{ wt}\%$ . Fractional crystallization is not evident from the Harker diagrams (Fig. 3a–d). The Agua Blanca and Cerro Colorado granites are peraluminous and subalkaline with 6.8 and 4.4 wt% corundum normative, respectively.

### 3.2.2. Trace and REE

The Agua Blanca and Cerro Colorado granites present restricted trace element concentrations, with Rb, Y, Nb, and Ga concentrations higher than those of the Meyer suite, whereas the Sr, Zr, and Ba concentrations are lower

(Fig. 3e–h). Logarithmic plots of Rb–Sr and Ba–Rb indicate restricted fractional crystallization of plagioclase and K-feldspar (Grecco et al., 1999). Total REE concentrations are between 104 and 177 ppm in Cerro Colorado and between 98 and 370 ppm in Agua Blanca. The chondrite-normalized diagram for the Cochenleufú suite indicates enrichments of 60–150 times in Cerro Colorado and 50–400 times in Agua Blanca (Fig. 4e and f). Both bodies have strong negative Eu anomalies with  $\text{Eu}/\text{Eu}^* = 0.049\text{--}0.094$  in Agua Blanca and 0.051–0.127 in Cerro Colorado. These anomalies indicate that plagioclase was severely fractionated from the original magma.

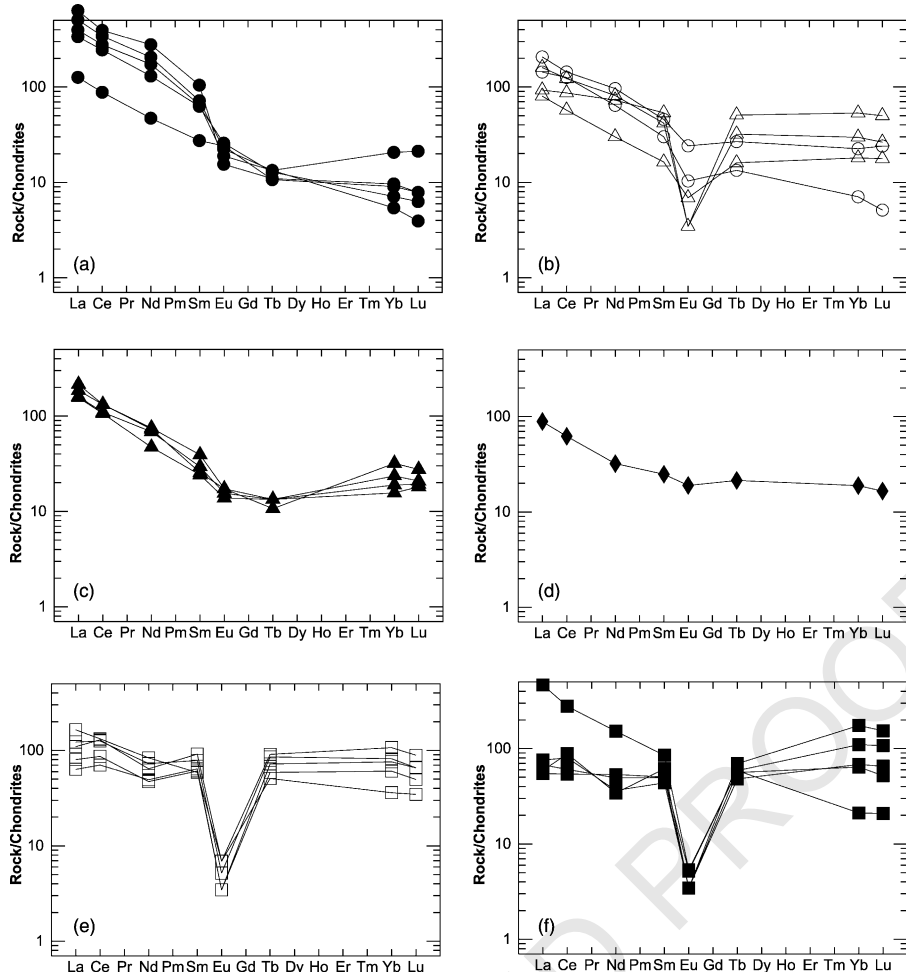


Fig. 4. Chondrite-normalized spider diagrams for (a) Pan de Azucar granite, (b) Cerro del Corral granite and rhyolites, (c) San Mario granite, (d) Pan de Azucar andesite, (e) Cerro Colorado granite, and (f) Agua Blanca granite. Symbols as in Fig. 3.

#### 4. Previous geochronological studies

Previous radiometric ages (Borrello and Venier, 1967; Cazeneuve, 1967; Cingolani and Varela, 1973; Varela and Cingolani, 1975; Rapela et al., 2001, 2003) using K/Ar, Rb/Sr, and U-Pb SHRIMP data have been determined for the granitic and volcanic rocks of Sierra de la Ventana (Fig. 5). Late Proterozoic ages were obtained for the Cerro del Corral rhyolite ( $671 \pm 35$ ,  $655 \pm 30$ ,  $638 \pm 30$  Ma), Cerro del Corral granite ( $612.3 \pm 5.3$ ,  $607 \pm 5.2$  Ma), Pan de Azucar andesite ( $603 \pm 30$  Ma), and Pan de Azucar granite (598 Ma).

Cingolani and Varela (1973) also constructed a Rb/Sr isochron using samples from both the San Mario and Agua Blanca granites to obtain an age of  $574 \pm 10$  Ma. Lower Paleozoic ages were obtained for the Cerro Colorado granite ( $487 \pm 15$ ,  $407 \pm 21$ ,  $529.6 \pm 3.3$ ,  $531.1 \pm 4.1$  Ma), Agua Blanca granite (492 Ma), San Mario granite ( $524.3 \pm 5.3$ ,  $526.5 \pm 5.5$  Ma), and La Ermita rhyolite ( $509 \pm 5.3$  Ma).

The age population indicates two magmatic cycles at 700–560 and 530–470 Ma, which are concordant with the field-, petrographical-, and geochemical-based separation

into two suites. Discrepancies arise when the younger age of the San Mario granite is compared with other members of the Meyer suite. However, zircon cores with ages that vary between 600 and 540 Ma and the Pb loss registered at 500 Ma suggest that the obtained age is not completely reliable, especially considering the strong similarities in the geochemistry, petrography, and deformation of the San Mario, Pan de Azucar, and Cerro del Corral granites. On this basis, the San Mario granite is included in the Meyer suite.

Equivalent magmatic cycles have been recognized in South Africa, where they constitute the Cape granite suite (Scheepers, 1995; Scheepers and Poujol, 2002).

#### 5. Tectonic discrimination

##### 5.1. Meyer suite

Pearce et al. (1984) subdivide the granitoids, according to their tectonic setting, into intrusion in ocean ridge, volcanic arc, within plate, orogenic, and syncollisional granites. In the Y + Nb versus Rb diagram (Fig. 6a),

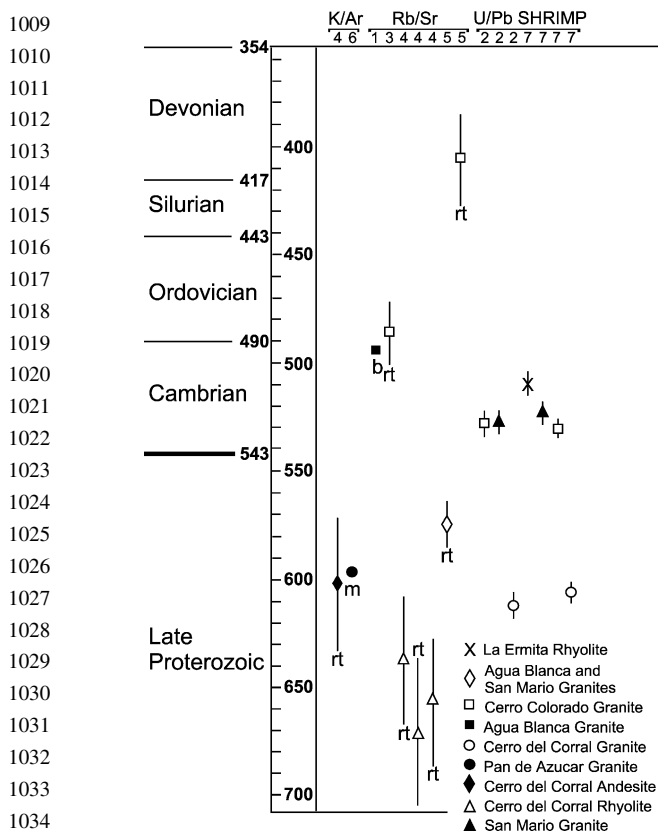


Fig. 5. Radiometric ages obtained from Sierra de la Ventana. (1) Borrello and Venier, 1967; (2) Rapela et al., 2001; (3) Varela et al., 1990; (4) Varela and Cingolani, 1975; (5) Cingolani and Varela, 1973; (6) Cazeneuve, 1967; and (7) Rapela et al., 2003. rt = whole rock, b = biotite, and m = muscovite.

samples plot dominantly in the volcanic arc field, whereas in the Y versus Nb diagram, they plot in both the volcanic arc and syncollisional fields (Fig. 6b).

Whalen et al. (1987) discriminate between A-type granites and most orogenic granitoids (M-, I-, and S-types) using the Ga/Al relationships and Y, Nb, and Zr concentrations. In Whalen et al.'s (1987) discrimination diagrams, the Meyer suite granites plot in the S- and I-type

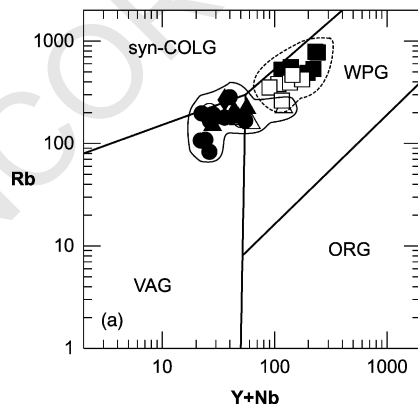


Fig. 6. (a) Rb versus Y + Nb diagram (Pearce et al., 1984) and (b) Y versus Nb diagram for the Meyer and Cochenleufú suites. Symbols as in Fig. 3.

granite fields (Fig. 7). These results indicate that the Meyer suite consists of S-type granites, as defined by Chappell and White (1974).

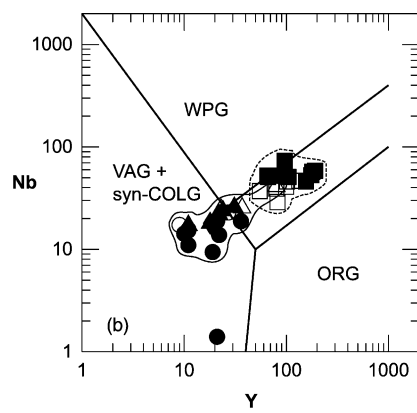
Harris et al. (1986) recognize four groups of granitic rocks in the Himalayan, Alpine, and Hercynian belts: (1) precollisional, calc-alkaline, dioritic to granodioritic plutons associated with volcanic arcs; (2) syncollisional, peraluminous leucogranites; (3) late- or postcollisional, calc-alkaline, biotite-hornblende tonalite to granodioritic plutons; and (4) postcollisional alkaline rocks. In the triangular diagram Rb/30-Hf-Ta\*3 (Fig. 8a), samples plot in the precollisional (volcanic arc) and the late- or postcollisional fields, though a few appear in the within-plate field. In the SiO<sub>2</sub> wt% versus Rb/Zr diagram (not shown), most samples plot in the VAG field. In the Y-Nb-Ce and Y-Nb-3\*Ga diagrams of Eby (1992), most samples plot in the A<sub>1</sub>-type granite field (Fig. 9a and b).

Rocks with geochemical and petrologic characteristics emplaced during a subduction-collision event have been recognized in the Karakoram Axial batholith of northern Pakistan (Baltoro plutonic unit, Hunza leucogranite; Crawford and Windley, 1990), the Pan-African belt of the Arabian shield (Jackson et al., 1984), the Homrit Wagat complex of Egypt (Hassanen, 1997), and the Qinling belt of China (Mattauer et al., 1985).

Through plotting in TiO<sub>2</sub>-MnO\*10-P<sub>2</sub>O<sub>5</sub>\*10, Ti/100-Zr-Y\*3, and Th/Yb-Ta/Yb discriminant diagrams (Pearce and Cann, 1973; Pearce, 1982; Mullen, 1983), the Pan de Azucar andesite is classified as a calc-alkaline basalt that erupted at active continental margins (not shown).

## 5.2. Cochenleufú suite

Samples from the Cochenleufú suite plot in the within-plate granite field (Fig. 6) of Pearce et al. (1984) diagrams. They also fall in the A-type granite field in trace elements versus 10000 Ga/Al discrimination diagrams (Fig. 7). This result agrees with the A-type granite characteristics of these rocks, namely, the high SiO<sub>2</sub>, Na<sub>2</sub>O + K<sub>2</sub>O, Ga/Al, Zr, Nb, Ga, Y, and Ce and low CaO.



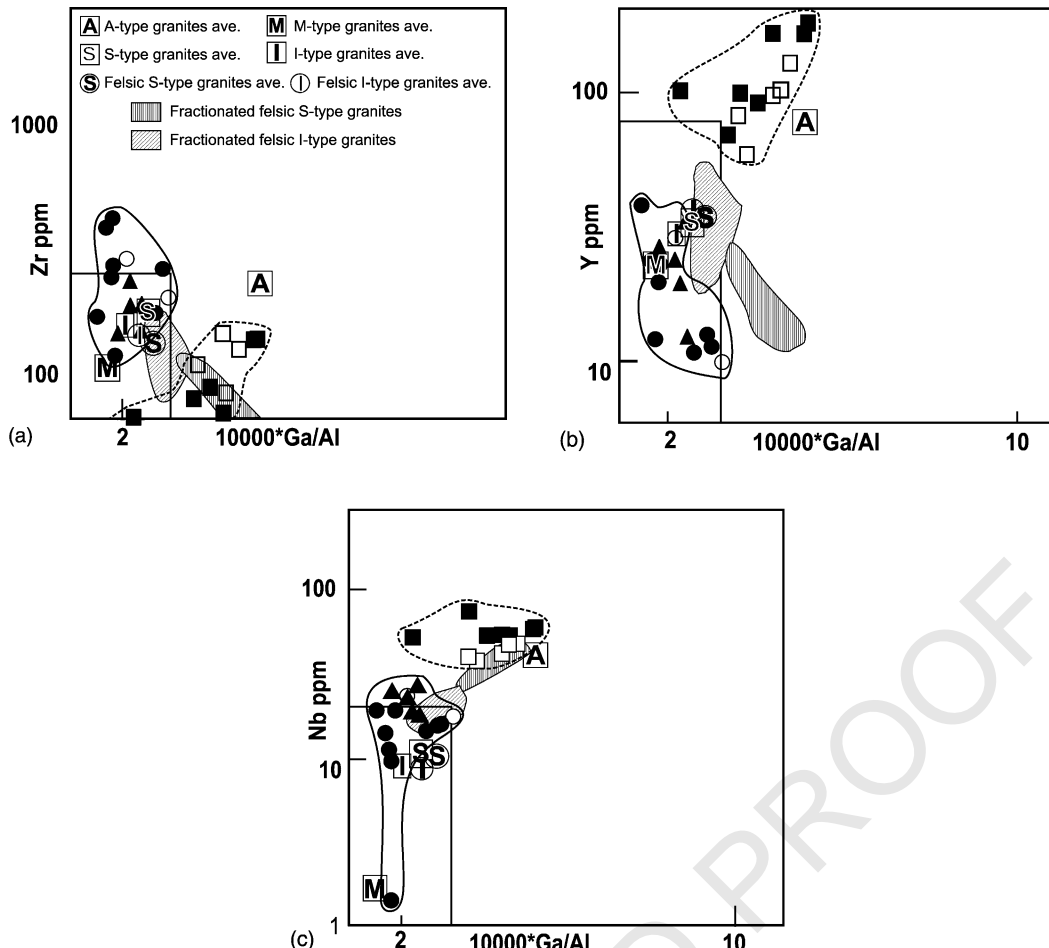


Fig. 7. (a) Zr, (b) Nb, and (c) Y versus  $10000 \text{ Ga/Al}$  diagrams (Whalen et al., 1987) for the Meyer and Cochenleufú suites. Symbols as in Fig. 3.

In the Rb/30-Hf-Ta\*3 diagram (Harris et al., 1986), the samples plot in the syn- to postcollisional fields (Fig. 8b); in the SiO<sub>2</sub> wt% versus Rb/Zr diagram (not shown), they are classified in the syncollisional field.

Finally, in Eby (1992) Y-Nb-Ce and Y-Nb-3\*Ga diagrams, most of the samples plot in the continental–continental collisional to postcollisional field (Fig. 9a and b). Examples include the Gabo and Mumbulla suites in the Lachland fold belt, Australia (Collins et al., 1982),

and the Topsails complex of Newfoundland (Whalen et al., 1987).

## 6. Discussion

In Sierra de la Ventana, the deficiency of igneous rock outcrops, as well as the lack of field relationships with host rocks, makes it difficult to establish its tectonic

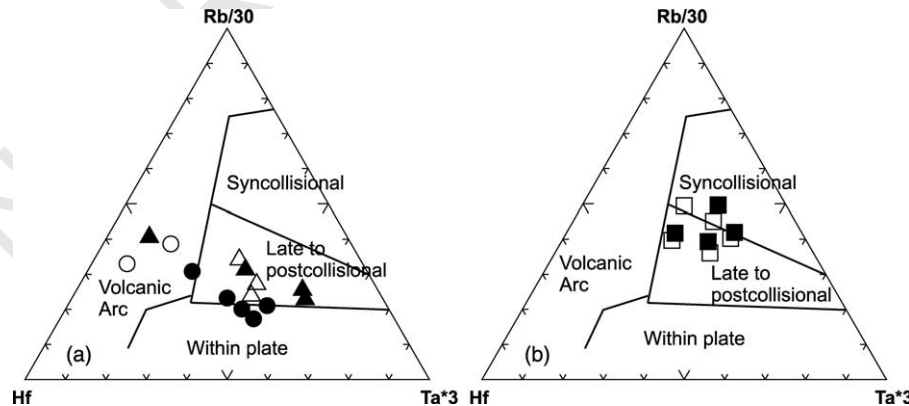


Fig. 8. Rb/30-Hf-Ta\*3 diagrams (Harris et al., 1986) for the (a) Meyer and (b) Cochenleufú suites. Symbols as in Fig. 3.

1233

1234

1235

1236

1237

1238

1239

1240

1241

1242

1243

1244

1245

1246

1247

1248

1249

1250

1251

1252

1253

1254

1255

1256

1257

1258

1259

1260

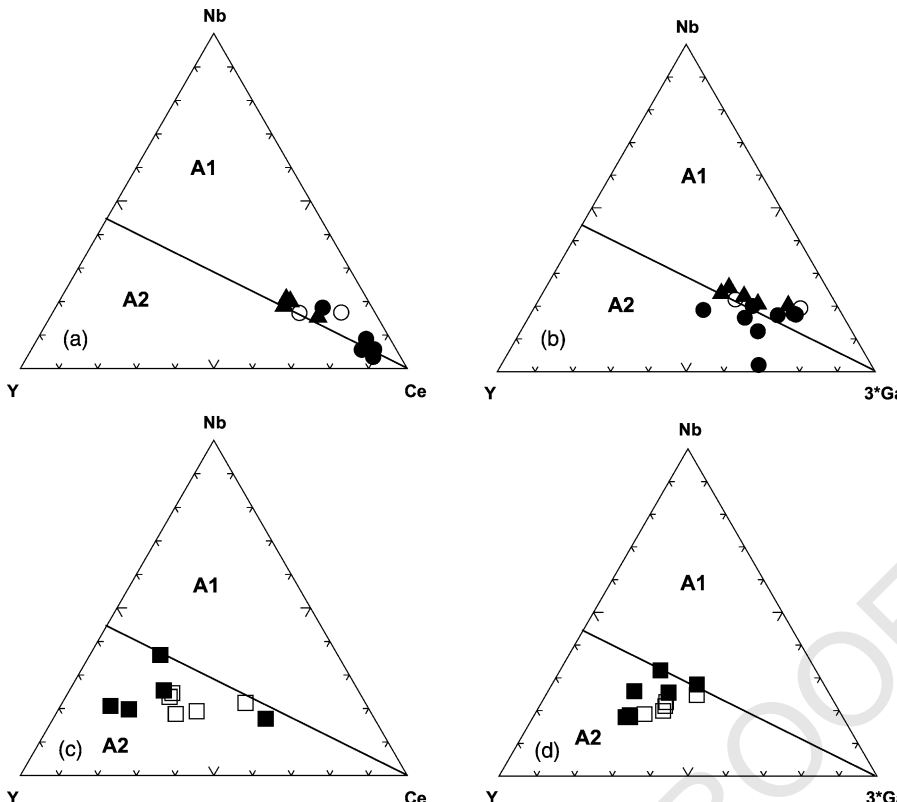


Fig. 9. (a, c) Y–Nb–Ce diagram (Eby, 1992) and (b, d) Y–Nb– $3^*Ga$  diagram for the Meyer and Cochenleufú suites. Symbols as in Fig. 3.

setting. However, the correlation with the African granitic suites enables us to clarify the evolution of accretional events in Sierra de la Ventana. Two igneous suites are differentiated in Sierra de la Ventana. The most basic is the Meyer suite (700–570 Ma), which displays a calc-alkaline evolution related to volcanic arc and postcollisional settings.

In the Saldania belt of South Africa, sedimentary and volcanic rocks deposited in the Boland terrane (Malmesbury Group) attest to ocean floor spreading in response to the breakup of Rodinia and the progressive opening of the proto-Atlantic (Adamastor Ocean) during 780–750 Ma (Rozendaal et al., 1999). Rocks of this age, which represent this extensional event, had not been recognized in Sierra de la Ventana, though they were found in Sierra de Tandil. A reversal of the spreading caused subduction and the closure of the Adamastor Ocean (600–570 Ma). The presence of a suture zone at the Swartland-Boland terrane boundary supports either oblique collision or strike-slip transpressional tectonics without the development of a proper collision orogen. The Cape granite suite consists of a first and second phase of intrusion (600–520 Ma), with olivine gabbros, gabbros, diorites, and granodiorites related to subduction along an immature magmatic arc (Scheepers, 1995). S-type granitic rocks that intruded during this phase have late orogenic to postorogenic signatures. In Sierra de la Ventana, the Meyer suite represents this subduction-collision event.

The Cochenleufú suite (540–470 Ma) is considered an A-type association and plots in the within-plate, syn- to postcollisional fields in several discrimination diagrams. According to Eby (1992) classification, these rocks belong to the A<sub>2</sub> granitoids, which generally occur as final plutonic events during postorogenic extension in collisional belts (Crawford and Windley, 1990; Bonin, 1990).

In the Cape granite suite, the final phase of intrusion (520–500 Ma) is represented by A-type granitoids (Scheepers, 1995), which are considered anorogenic alkaline granites. The granites are related to the pressure release that occurs during a strike-slip regime, with associated uplift and extension after collision. Equivalent postcollisional granites, intruded during an oblique N–S collision of the Kalahari and Congo cratons, have been recognized in the central Damaran orogenic belt, Namibia (Gresse and Scheepers, 1993). They are related to the closure of the Adamastor Ocean.

The Swartland and Tygerberg terranes (Saldania belt), accreted in a transpressive regime to the Boland terrane (600–630 Ma), are potential candidates for the Sierra de la Ventana suites' emplacement.

Similar structural styles, magmatism, and tectonic events have been recognized in the Saldania, Ross, and Delamarian orogens, indicating a common history (Rozendaal et al., 1999). The Ross event, responsible for major magmatism in the Transantarctic Mountains, is represented partially by the granitic Harbour intrusive complex (Gunn and Warren,

1345 1962), which was emplaced in a calc-alkaline arc. The Mid-  
 1346 Proterozoic-Late Cambrian history of the Transantarctic  
 1347 Mountains has been interpreted as a cycle of extension,  
 1348 continental rifting, transpression, and subduction (Moyes  
 1349 et al., 1993).

1350

## 1351 7. Conclusions

1354 In Sierra de la Ventana, two magmatic suites are  
 1355 differentiated. The older Meyer suite (700–570 Ma) displays  
 1356 a calc-alkaline evolution related to a volcanic arc and  
 1357 postcollisional setting. The younger Cochenleufú suite  
 1358 (540–470 Ma) displays an A-type signature related to  
 1359 the final plutonic events during postorogenic extension in  
 1360 the collisional belts.

1361 The remarkable similarities observed between the suites  
 1362 of Sierra de la Ventana and the Saldania belt enables a  
 1363 positive correlation. In both cases, primitive volcanic arc or  
 1364 collisional orogens are recognized. Moreover, continuous  
 1365 shearing between the Swartland and Tygerberg terranes was  
 1366 a potential trigger for the emplacement of both suites.

## 1368 8. Uncited reference

1370 Varela and Cingolani, 1990.

## 1373 Acknowledgements

1375 We thank V. Ramos (UBA), E. Llambías (UNLP), and  
 1376 I. Petrinovic (UNSa) for reviews and comments on an early  
 1377 draft of the manuscript. We also thank José L. Fernandez  
 1378 Turiel for helping during X-ray fluorescence analyses.  
 1379 A Marie Curie bursary of the European Community to DAG  
 1380 supported part of this research.

## 1383 References

- 1385 Andreis, R.R., 1964. Petrología del Grupo eodevónico de Lolén. Sierras  
 1386 Australes de la Provincia de Buenos Aires. Com. Investig. Científicas.  
 1387 Anal. 5, 79–124.La Plata.
- 1388 Andreis, R.R., Iñiguez Rodríguez, A.M., Lluch, J., Rodríguez, S., 1989.  
 1389 Cuenca paleozoica de Ventania. Sierras Australes de la provincia de  
 1390 Buenos Aires. In: Chebli, G., Spalletti, L. (Eds.), Cuenca Sedimentarias Argentinas. Serie Correlación Geológica, Univ. Nac. Tucumán,  
 1391 pp. 265–298.
- 1392 Bonin, B., 1990. From orogenic to anorogenic settings: evolution of  
 1393 granitoid suites after a major orogenesis. Geol. J. 25, 261–270.
- 1394 Borrello, A.V., 1962. Sobre los niveles fosilíferos del Devónico inferior de  
 1395 las Sierras Australes de la Provincia de Buenos Aires. Notas Comisión  
 1396 de Investigaciones Científicas I, 4. La Plata.
- 1397 Borrello, A.V., 1964. Los geosinclinales de la Provincia de Buenos Aires.  
 1398 GAEA, Soc. Argentina de Est. Geográficos, Anales XII, 9–19. Buenos  
 1399 Aires.
- 1400 Borrello, A., Venier, J., 1967. Nuevas características geológicas del granito  
 Agua Blanca, Dufaur. Prov. de Bs. As. Notas Comisión de  
 1400 Investigaciones Científicas 2, pp. 3–7.
- Buggisch, W., 1987. Stratigraphy and very low-grade metamorphism of  
 1401 the Sierras Australes de la Provincia de Buenos Aires (Argentina)  
 1402 and implications in Gondwana correlation. Zentral. Geol. Palaont. Teil I  
 1403 7/8, 819–837.
- Cazeneuve, H., 1967. Edades isotópicas del basamento de la provincia  
 1404 de Buenos Aires. Ameghiniana. Rev. Asoc. Paleont. Arg. 5 (1),  
 1405 3–10.
- Chappell, B.W., White, A.J.R., 1974. Two contrasting granite types. Pacific  
 1406 Geol. 8, 173–174.
- Cingolani, C.A., Varela, R., 1973. Examen geocronológico por el método  
 1407 rubidio-estróncio de las rocas ígneas de las Sierras Australes  
 1408 bonaerenses. V Congr. Geol. Arg. Actas 1, 349–371.
- Cobbbold, P.R., Massabie, A.C., Rossello, E.A., 1986. Hercynian wrenching  
 1411 and thrusting in the Sierras Australes Foldbelt, Argentin. Hercynia 2  
 1412 (2), 135–148.
- Collins, W.J., Beams, S.D., White, A.J.R., Chappell, B.W., 1982. Nature  
 1413 and origin of A-type granites with particular reference to Southeastern  
 1414 Australia. Contrib. Miner. Petrol. 80, 187–200.
- Crawford, M.B., Windley, B.F., 1990. Leucogranites of the Himalaya/  
 1415 Karakoram: implications for magmatic evolution within collisional  
 1416 belts and the study of collision-related leucogranite petrogenesis.  
 1417 J. Volcanol. Geoth. Res. 44, 1–19.
- Cucchi, R.J., 1966. Petrofábrica del conglomerado de la Formación La  
 1418 Lola, Sierras Australes de la Provincia de Buenos Aires. Rev. Asoc.  
 1419 Geol. Arg. 21, 71–106.
- Cuerda, A.J., Cingolani, C.A., Barraquero, H.R., 1975. Estratigrafía del  
 1420 Basamento Precámbrico en la Comarca de los Cerros Pan de Azucar-del  
 1421 Corral, Sierras Australes (Provincia de Buenos). II Congr. Iberoam.  
 1422 Geol. Económ II, 57–63.Buenos Aires.
- Delpino, S., Dimieri, L., 1992. Características de la deformación y  
 1423 cinemática de las rocas del basamento, perfil Las Lomitas, Sierras  
 1424 Australes de Buenos Aires. VIII Reunión de Microtectónica, Actas,  
 1425 11–14.Bariloche.
- Dimieri, L., Grecco, L., Friscale, C., 1990. Microestructuras en el Granito  
 1426 Aguas Blancas, Provincia de Buenos Aires, Argentina. Rev. Asoc. Arg.  
 1427 Miner. Petrol. y Sediment. 21 (1–4), 53–60.
- Du Toit, A.L., 1937. Our wandering continents. Oliver Boyd, Edinburg,  
 1428 p. 366.
- Eby, G.N., 1992. Chemical subdivision of the A-type granitoids:  
 1429 petrogenetic and tectonic implications. Geology 20, 641–644.
- Grecco, L.E., 1990. Geoquímica y Petrología de los intrusivos graníticos  
 1430 Cerros Colorados y Aguas Blancas, Sierras Australes, Provincia de  
 1431 Buenos Aires. Unpublished PhD Thesis, Universidad Nacional del Sur,  
 1432 Bahía Blanca, p. 159.
- Grecco, L.E., Gregori, D.A., 1993. Estudio geoquímico de los intrusivos  
 1433 graníticos Cerros Colorados y Aguas Blancas, Sierras Australes de la  
 1434 provincia de Buenos Aires, Argentina. XII Congr. Geol. Arg. y II  
 1435 Congr. Explor. Hidrocarburos, Actas IV, 81–89.Buenos Aires.
- Grecco, L.E., Gregori, D.A., Maiza, P.J., 1984. Relación del contenido de  
 1436 flúor y de OH en las biotitas de las rocas graníticas de la cantera Cerros  
 1437 Colorados Provincia de Buenos Aires. IX. Congr. Geol. Arg., Actas 3,  
 1438 368–375.
- Grecco, L.E., Gregori, D.A., Ruviños, M.A., 1999. Characteristics of  
 1439 Neoproterozoic magmatism in Sierras Australes. Zentral. Geol.  
 1440 Palaontol. H3-6, 609–619.
- Gresse, P.G., Scheepers, R., 1993. Neoproterozoic to Cambrian (Namibian)  
 1441 rocks of South Africa: a geochronological and geotectonic review.  
 1442 J. African Earth Sci. 16 (4), 375–393.
- Gunn, G.M., Warren, G., 1962. Geology of Victoria Land between the  
 1443 Mawson and Mullock Glaciers, Antarctica. NZ Geol. Surv. Bull. 71,  
 1444 157.
- Harrington, H.J., 1947. Explicación de las Hojas Geológicas 33m y 34m  
 1445 Sierras de Curamalal y de la Ventana, Provincia de Buenos Aires. Serv.  
 1446 Nac. Min. Geol. Bol. 61, 46Buenos Aires.
- Harrington, H.J., 1970. Las Sierras Australes de Buenos Aires, República  
 1447 Argentina: Cadena Aulacogénica. Rev. Asoc. Geol. Arg. 25 (2),  
 1448 151–181.

- 1457 Harrington, H.J., 1972. Sierras Australes de Buenos Aires. Geología  
1458 Regional Argentina. Acad. Nac. Cs. Córdoba, 395–405.Buenos Aires.
- 1459 Harrington, H.J., 1980. Sierras Australes de la Provincia de Buenos Aires.  
1460 Segundo Simposio de Geología Regional Argentina. Acad. Nac. Cs 2,  
967–983.
- 1461 Harris, N.B.W., Pearce, J.A., Tindle, A.G., 1986. Geochemical character-  
1462 istics of collision-zone magmatism. In: Coward, M.P., Ries, A.C. (Eds.),  
1463 Collision Tectonics, Geol. Soc. Special Publications, vol. 18., pp. 67–81.
- 1464 Hassanan, M.A., 1997. Post-collision, a-type granites of Homrit Wagat  
complex, Egypt: petrological and geochemical constraints on its origin.  
1465 Precambrian Res. 82, 211–236.
- 1466 Iñiguez Rodríguez, A.M., Andreis, R.R., 1971. Caracteres sedimentológi-  
1467 cos de la Formación Bonete, Sierras Australes de la Provincia de  
1468 Buenos Aires. Reunión Geol. Sierras Australes Bonaerenses, Prov.  
Buenos Aires, Com. Investig Científicas, 103–120.La Plata.
- 1469 Jackson, N.J., Walsh, J.N., Pegram, E., 1984. Geology, geochemistry and  
1470 petrogenesis of late Precambrian granitoids in the Central Hijaz region  
1471 of the Arabian Shield. Contrib. Miner. Petrol. 87, 205–219.
- 1472 Keidel, J., 1916. La geología de las sierras de la Provincia de Buenos Aires  
y sus relaciones con las montañas de Sud-Africa y los Andes. Anales del  
1473 Ministerio de Agricultura de la Nación. Dir. Geol., Miner. Min. 9 (3),  
1–78.
- 1475 Kilmurray, J.O., 1968a. Petrología de las rocas cataclásicas y el skarn del  
1476 anticlinal del Cerro Pan de Azúcar (Partido de Saavedra Provincia de  
1477 Buenos Aires). Terceras Jorn. Geol. Arg. Acta Lilloaillana 6, 217–238.
- 1478 Kilmurray, J.O., 1968b. Petrología de las rocas ígneas de las Sierras Australes  
de la Prov. de Bs. As. Revista Museo de La Plata 6 (45), 155–188.
- 1479 Kilmurray, J.O., 1975. Las Sierras Australes de la Provincia de Buenos  
Aires, las facies de deformación y nueva interpretación estratigráfica.  
1480 Rev. Asoc. Geol. Arg. 30 (4), 331–348.
- 1481 Kilmurray, J.O., Leguizamón, M.A., Teruggi, M.E., 1985. Caracteres  
1482 estructurales y petrológicos de la Formación Trocadero en las abras de  
Agua Blanca, abra de Hinojo y Sofía, Sierras Australes de la provincia  
1483 de Buenos Aires. I Jorn. Geol. Bonaerenses, 228.
- 1484 Leat, P.T., Jackson, S.E., Thorpe, R.S., Stillman, C.J., 1986. Geochemistry  
1485 of bimodal basalt-subalkaline/peralkaline rhyolite provinces within the  
Southern British Caledonides. J. Geol. Soc. London 143, 259–273.
- 1486 Llambías, J.E., Prozzi, C.R., 1975. Ventania. Relatorio VIº Congr. Geol.  
1487 Arg. B, 79–102.Buenos Aires.
- 1488 Mattauer, M., Matte, Ph., Malaville, J., Tapponnier, P., Maluski, H., Qin,  
1489 X.Z., Lun, L.Y., Qin, T.Y., 1985. Tectonics of the Qinling belt: build-up  
and evolution of eastern Asia. Nature 317, 496–500.
- 1490 Miller, R.B., Paterson, S.R., 1994. The transition from magmatic to high-  
1491 temperature solid-state deformation: implications from the Mount  
Stuart batholith Washington. J. Struct. Geol. 16, 853–865.
- 1492 Moyes, A.B., Barton, J.M. Jr, Groenewald, P.B., 1993. Late Proterozoic to  
1493 Early Paleozoic tectonism in Dronning Maud Land Antarctica:  
1494 Supercontinental fragmentation and amalgamation. J. Geol. Soc.  
London 150, 833–842.
- 1495 Mullen, E.D., 1983. MnO/TiO<sub>2</sub>/P<sub>2</sub>O<sub>5</sub>: a minor element discriminant for  
1496 basaltic rocks of oceanic environments and its implications for  
petrogenesis. Earth Planet. Sci. Lett. 62, 53–62.
- 1497 Paterson, S.R., Vernon, R.H., Tobisch, O.T., 1989. A review of criteria for  
1498 the identification of magmatic and tectonic foliations in granitoids.  
J. Struct. Geol. 11 (3), 349–363.
- 1499 Pearce, J.A., 1982. Trace element characteristics of lavas from destructive  
1500 plate boundaries. In: Thorpe, R.S., (Ed.), Andesites: Orogenic  
Andesites and Related Rocks, Wiley, Chichester, pp. 525–548.
- 1501 Pearce, J.A., Cann, J.R., 1973. Tectonic setting of basic volcanic rocks  
1502 determined using trace element analyses. Earth Planet. Sci. Lett. 19,  
290–300.
- 1503 Pearce, J.A., Harris, N.B.W., Tindle, A.G., 1984. Trace element  
1504 discrimination diagrams for the tectonic interpretation of granitic  
rocks. J. Petrol. 25, 956–983.
- 1505 Pecerrillo, A., Taylor, S.R., 1976. Geochemistry of Eocene calcoalkaline  
1506 volcanic rocks from the Kastamonu Area, northern Turkey. Contrib.  
1507 Miner. Petrol. 58, 63–81.
- 1508 Rapela, C.W., Pankhurst, R.J., 2002. Eventos tecto-magmáticos del  
1509 Paleozoico inferior en el margen Proto-Atlántico del Sur de  
Sudamérica. XV Congr. Geol. Arg. Actas, 24–29.
- 1510 Rapela, C.W., Pankhurst, R.J., Fanning, C.M., 2001. U–Pb SHRIMP ages  
1511 of basement rocks from Sierra de la Ventana (Buenos Aires province,  
Argentina). III South American Symp. Isotope Geol. Actas (CD),  
Pucón, Chile.
- 1512 Rapela, C.W., Pankhurst, R.J., Fanning, C.M., Grecco, L.E., 2003.  
1513 Basement evolution of the Sierra de la Ventana fold belt: new evidence  
1514 for Cambrian continental rifting along the southern margin of  
Gondwana. J. Geol. Soc. London 160, 613–628.
- 1515 Rozendaal, A., Gresse, P.G., Scheepers, R., Le Roux, J.P., 1999.  
1516 Neoproterozoic to Early Cambrian crustal evolution of the Pan-African  
Saldanía belt. South Africa Precambrian Res. 97 (3–4), 303–323.
- 1517 Scheepers, R., 1995. Geology and petrogenesis of the Late Precambrian S-,  
1518 I-, and A-type granitoids in the Saldanía belt, Western Cape Province,  
1519 South Africa. J. African Earth Sci. 21, 35–58.
- 1520 Schiller, W., 1930. Investigaciones Geológicas en las montañas del  
1521 Sudoeste de la Provincia de Buenos Aires. Anales del Museo de la  
Plata. Sección Mineral. Geol. Segunda Serie (primera parte) 4,  
9–101.La Plata.
- 1522 Sellés Martínez, J., 1989. The structure of Sierras Australes (Buenos Aires,  
1523 Argentina). An example of folding in a transpressive environment.  
J. South Am. Earth Sci. 2 (4), 317–329.
- 1524 Shand, S.J., 1943. Eruptive rocks: Their Genesis, Composition, Classifi-  
cation, and Their Relations to Ore-Deposits. Wiley, New York.
- 1525 Simpson, C., 1985. Deformation of granitic rocks across the ductile-brittle  
transition. J. Struct. Geol. 7, 503–511.
- 1526 Tribe, I.R., D'Lemos, R.S., 1996. Significance of a hiatus in down-  
1527 temperature fabric development within syn-tectonic quartz diorite  
complexes, Channel Islands, UK. J. Geol. Soc. London 153, 127–138.
- 1528 Varela, R., 1973. Edad Rb/Sr de las rocas ígneas de La Mascota–La Ermita,  
1529 partido de Saavedra, Provincia de Buenos Aires. Anal. Soc. Científica  
Arg. CXCV (I–II), 71–80.
- 1530 Varela, R., 1978. Sierras Australes de la Provincia de Buenos Aires:  
1531 Hipótesis de trabajo sobre su composición geológica y rasgos  
geotectónicos salientes. Rev. Asoc. Geol. Arg. 33 (1), 52–62.
- 1532 Varela, R., Cingolani, C., 1975. Nuevas edades radimétricas del basamento  
1533 aflorante en el Perfil del Cerro Pan de Azúcar–Cerro del Corral y  
consideraciones sobre la evolución geocronológica de las rocas ígneas  
1534 de las Sierras Australes, Provincia de Buenos Aires. VI Congr. Geol.  
Arg. Actas I, 543–556.
- 1535 Varela, R., Cingolani, C.A., 1990. Edad del granito del Cerro Colorado y su  
1536 implicancia geotectónica. Sierras Australes de Buenos Aires. XI Congr.  
Geol. Arg. Actas II, 279–282.Buenos Aires.
- 1537 Varela, R., Dalla Salda, L.H., Cingolani, C.A., 1985. Estructura y  
1538 composición geológica de las sierras Colorada, Chasicó y Cortapié,  
Sierras Australes de Buenos Aires. Rev. Asoc. Geol. Arg. 40 (3–4),  
254–261.
- 1539 von Gosen, W., 2002. Polyphase structural evolution in the northeastern  
1540 segment of the North Patagonian Massif (Southern Argentina). J. South  
Am. Earth Sci. 15, 591–623.
- 1541 von Gosen, W., Buggisch, W., Dimieri, L., 1990. Structural and  
1542 metamorphic evolution of Sierras Australes (Buenos Aires Province  
Argentina). Geologische Rundschau 79/3, 797–821.
- 1543 von Gosen, W., Buggisch, W., Krümm, S., 1991. Metamorphic and  
1544 deformation mechanisms in the Sierras Australes fold thrust belt  
(Buenos Aires Province Argentina). Tectonophysics 185, 335–356.
- 1545 Whalen, J.B., Currie, K.L., Chappell, B.W., 1987. A-type granites:  
1546 Geochemical characteristics, discrimination and petrogenesis. Contrib.  
Miner. Petrol. 95, 407–419.
- 1547 Winchester, J.A., Floyd, P.A., 1977. Geochemical discrimination of  
1548 different magma series and their differentiation products using  
immobile elements. Chem. Geol. 20, 325–343.